



Behavior of thermoelectric generators exposed to transient heat sources



Nguyen Q. Nguyen, Kishore V. Pochiraju*

Design & Manufacturing Institute, Department of Mechanical Engineering, Stevens Institute of Technology, Castle Point on Hudson, Hoboken, NJ 07030, USA

HIGHLIGHTS

- Thermoelectric model with Peltier, Seebeck, Joule and Thomson effects.
- Thomson effects are shown to play a significant role in power generation modes.
- Optimal operating points for generating power from transient heat sources.

ARTICLE INFO

Article history:

Received 20 October 2011

Accepted 25 August 2012

Available online 12 September 2012

Keywords:

Thermoelectric generators
Direct energy conversion
Dynamic transient analysis
Thomson coefficient effect
Thermoelectric coupling physics
Characterization of thermal–electrical properties

ABSTRACT

This paper describes the power generation behavior of a thermoelectric generator (TEG) exposed to a transient heat source on the hot side and natural convection on the cold side. The simulation situation is typical in energy harvesting applications. Modeling thermoelectric generators (TEGs) under these conditions is complicated compared to thermoelectric coolers because of the non-linearities and the unknown electric currents in a closed-loop circuit. A transient thermoelectric model that includes Seebeck, Peltier, Thomson, and Joule effects is solved using finite-difference techniques and the power generated from a TEG is simulated. Using open-circuit experiments were used to establish key parameters governing the thermal behavior and thermoelectric coupling. Experiments with closed-circuits and load resistors were used to validate the model. The results show that inclusion of Thomson effect plays a significant role in accurately predicting the power generated by the device.

© 2012 Elsevier Ltd. All rights reserved.

1. Introduction

Thermoelectric generators (TEGs), or Seebeck elements, enable conversion of thermal energy into electricity without any moving parts. The Seebeck elements can be used for temperature sensing and power generation applications [1]. TEGs generate electric current in a closed-circuit across a load when a temperature gradient develops between the two ends of the device [2–4]. The coupling effects governing the conversion are the Seebeck, Peltier, Thomson, and Joule effects.

Understanding the transient behavior of TEG is important for optimizing energy harvesting from waste heat, when one junction is exposed to an unsteady heat source and the other junction is subjected to natural convection at ambient temperature. Several models have been developed for such configurations [5–7], but most models assume either an unlimited heat source or steady state operational scenarios. Practical applications such as parasitic energy harvesting

from waste heat sources generally have unsteady heat flux and/or temperature conditions on the hot side of the TEG and pose a fully coupled thermoelectric problem [8]. Simulation of TEGs operating in transient mode is more challenging than the thermoelectric coolers (TECs) because both the temperature field and the electric currents vary with time. The problem is more simplified for TECs as a constant and known electric current is applied as input and only the temperature gradients need to be determined.

Several models for TEG modules can be found in the literature. Numerous analytical [6,9] and numerical [10–13] steady state models exist for simulation of TEGs. However, fully coupled and complete transient analyses are seldom presented. Transient analysis of TEG subjected to a load change from steady state configuration has been conducted using commercial software [14,15]. Mittrani et al. [16] considered temperature-dependent material properties and the effect of thermal and electrical contacts. Furthermore, most models exclude the Thomson effects [17,18] and their influence on apparent Seebeck coefficients. Crane [19] showed the differences in the TEG behavior at steady state and during transients using an uncoupled thermoelectric model that used a constant current value in the thermal balance equation and no Thomson effects.

* Corresponding author. Tel.: +1 201 216 8232/8053; fax: +1 201 216 8963.

E-mail addresses: nnguyen@stevens.edu (N.Q. Nguyen), kishore.pochiraju@stevens.edu (K.V. Pochiraju).

Nomenclature		t	Time coordinate
L	Length of p–n	x	Spatial coordinate
L_1	Thickness of ceramic hot plate	R	Internal resistance
L_2	Thickness of ceramic cold plate	R_0	Load resistance
A	Cross-sectional area	I	Electric current
A_s	Convection area of heat sink	V	Voltage
k	Thermal conductivity	\dot{Q}	Heat rate
ρ	Material density	W	Stored energy
C	Specific heat capacity	h	Film coefficient of heat sink
α	Seebeck coefficient	Subscripts	
μ	Thomson coefficient	p	p-type material
π	Peltier coefficient	n	n-type material
ε	Electrical resistivity	1	Material of hot plate
T	Temperature	2	Material of cold plate
T_∞	Ambient temperature		

In this paper, we examined the behavior of a TEG when exposed to unknown and varying heat source representative of energy harvesting scenarios. We simulated the power generation characteristics of the TEG under specified temperature profiles that emulate varying heat flux applied to the hot side. The model parameters for a commercial TEG element were characterized by correlating the simulation results and the experimental observations. We show that the developed numerical model captures the thermal behavior and the electrical behavior of the TEG in both open and closed-circuit configurations.

2. Theoretical modeling

2.1. Assumptions

The basic assumptions made include neglecting heat losses due to radiation and transverse convection. The flow of heat and current in the TEG is assumed one-dimensional. All materials are assumed homogeneous. Material property anisotropy is taken into account by selecting properties relevant along the dimension selected for the analysis. Thermal conductivities, electrical resistivity, and specific heat capacities of materials are assumed constant within the operating temperature range. While the numerical methods used did not require any of the above assumptions, these simplifications help in understanding the fundamental mechanisms. The reduction in the dimensionality of parametric space enhances the clarity during the correlation of experimental observations and model findings.

2.2. Governing equations

The schematic of a thermoelectric generator consisting of two thermoelectric elements, p- and n-type is shown in Fig. 1. The simulation dimension is divided into three local frames, namely $\{x_1, x, x_2\}$. The x -coordinate is chosen with the origin at the bottom surface of the TEG. The length of the TEG is denoted by L . x_1 and x_2 are local coordinates in the hot and cold plates at either ends of the TEG elements, respectively. The power at each junction induced by the Seebeck and Peltier effects and direction of thermal conduction through the two elements is shown in the figure. The current, $I(t)$, flowing through a load resistor indicates that the device is operating in power generation mode.

Governing equations for p- and n-thermoelectric elements are derived from the energy balance equation for an infinitesimal element, dx , as given in Eqs. (1) and (2) [17,20]:

$$A_p C_p \rho_p \frac{\partial T_p}{\partial t} = k_p A_p \frac{\partial^2 T_p}{\partial x^2} + \frac{\varepsilon_p}{A_p} I^2 - \mu_p I \frac{\partial T_p}{\partial x} \quad (1)$$

$$A_n C_n \rho_n \frac{\partial T_n}{\partial t} = k_n A_n \frac{\partial^2 T_n}{\partial x^2} + \frac{\varepsilon_n}{A_n} I^2 + \mu_n I \frac{\partial T_n}{\partial x} \quad (2)$$

where A_j , C_j , ρ_j , k_j , ε_j , μ_j and T_j are the cross-sectional area, specific heat capacity, density, thermal conductivity, electrical resistivity, Thomson coefficient and temperature of material j , respectively. I is the electric current flowing in a closed-circuit. t is the time variable and x is the spatial coordinate. Subscripts p and n denote the two TEG elements.

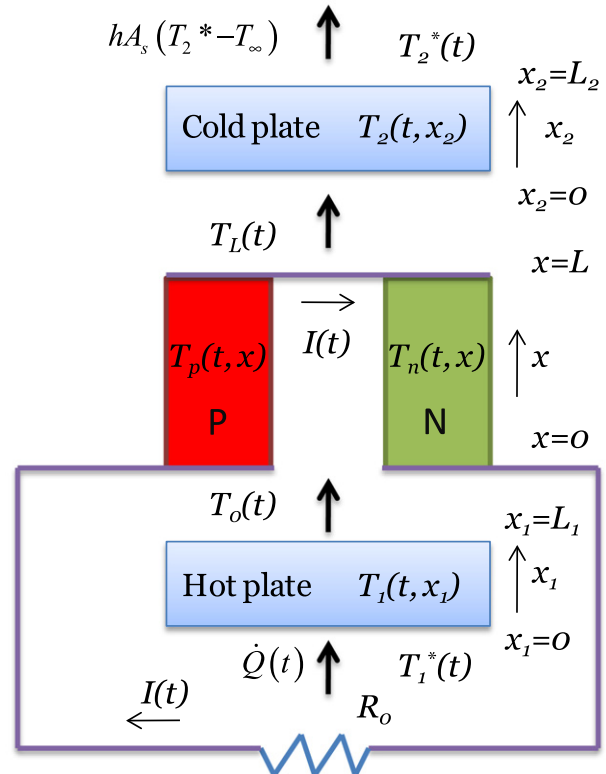


Fig. 1. Schematic of thermoelectric generators with hot and cold plates.

In contrast to an earlier model [20], we considered that the thickness of the hot and cold plates is in the same order of magnitude as the thermoelectric elements. The temperature field of these plates is also solved simultaneously with those of thermoelectric elements. Governing thermal balance equations of hot and cold plates are shown in Eq. (3) with subscript $j = 1$ for the hot plate and 2 for the cold plate.

$$\rho_j C_j \frac{\partial T_j}{\partial t} = k_j \frac{\partial^2 T_j}{\partial x_j^2} \quad (3)$$

2.3. Initial conditions

The initial temperature fields of elements are set to the ambient temperature, T_∞ . The subscript j indicates the material domain with $j = 1, 2, p$ or n denoting the hot, cold and the two TEG segments, respectively.

$$T_j(0, x_j) = T_\infty \quad (4)$$

2.4. Boundary and interface continuity conditions

The boundary condition applied at the bottom surface, $x_1 = 0$, corresponds to the applied unsteady heating rate, $\dot{Q}(t)$. The top surface, $x_2 = L_2$, has the film convection boundary condition employed. At the interfaces between two materials, $x_1 = L_1$ or $x = 0$ and $x = L$ or $x_2 = 0$, both the temperature and heat flux are assumed continuous implying a perfect bond between the TEG elements and the hot/cold plates.

$$x_1 = 0 \quad \dot{Q}(t) = -A_1 k_1 \frac{\partial T_1}{\partial x_1}(t, 0) \quad (5)$$

$$x_1 = L_1 (x = 0) \quad T_1(t, L_1) = T_p(t, 0) = T_0(t) \quad (6)$$

$$x_1 = L_1 (x = 0) \quad T_1(t, L_1) = T_n(t, 0) \quad (7)$$

$$\begin{aligned} x_1 = L_1 (x = 0) \quad & -A_1 k_1 \frac{\partial T_1}{\partial x_1}(t, L_1) \\ & = \alpha_{pn} T_0(t) I(t) - k_p A_p \frac{\partial T_p}{\partial x}(t, 0) - k_n A_n \frac{\partial T_n}{\partial x}(t, 0) \end{aligned} \quad (8)$$

$$x_2 = 0 (x = L) \quad T_p(t, L) = T_2(t, 0) = T_L(t) \quad (9)$$

$$x_2 = 0 (x = L) \quad T_n(t, L) = T_2(t, 0) \quad (10)$$

$$\begin{aligned} x_2 = 0 (x = L) \quad & \left(-\alpha_{pn} T_L(t) I(t) + k_p A_p \frac{\partial T_p}{\partial x}(t, L) + k_n A_n \frac{\partial T_n}{\partial x}(t, L) \right) \\ & = -A_2 k_2 \frac{\partial T_2}{\partial x_2}(t, 0) \end{aligned} \quad (11)$$

$$x_2 = L_2 \quad -A_2 k_2 \frac{\partial T_2}{\partial x_2}(t, L_2) = h A_s (T_2(t, L_2) - T_\infty) \quad (12)$$

with

$$\alpha_{pn} = \alpha_p - \alpha_n \quad (13)$$

In Eqs. (6)–(12), T_0 and T_L are the temperatures at the junctions $x = 0$ and $x = L$, respectively. h and A_s are the convection film coefficient and surface area of the top plate, respectively. A_1 and A_2 are the cross-sectional areas of hot and cold plates for a single p–n

unit cell, respectively. These values are obtained by dividing the plate area by the number of p–n units in the TEG.

2.5. Voltage generation in TEG

In the closed-circuit mode, the output voltage generated is computed as per Eq. (14):

$$V = V_{emf} - IR \quad (14)$$

with

$$V_{emf} = T_0 \alpha_{pn}(T_0) - T_L \alpha_{pn}(T_L) \quad (15)$$

$$R = \frac{\varepsilon_p L}{A_p} + \frac{\varepsilon_n L}{A_n} \quad (16)$$

The open-circuit voltage, V_{emf} , and the internal resistance of the Seebeck element are given by Eqs. (15) and (16). With a resistive load, R_0 , electric current (I) in the loop can be determined using Eq. (17).

$$I = \frac{V_{emf}}{R_0 + R} \quad (17)$$

We assume that Thomson coefficients of the p and n type of TEG elements are both independent of temperature [21]. The apparent Seebeck coefficient is taken to be related to the Thomson coefficients through the Kelvin relationship as given in Eq. (18).

$$\alpha_j(T) = \alpha_j^{\text{ref}} + \mu_j \ln(T/T_{\text{ref}}) \quad (18)$$

In this equation α_j^{ref} is the Seebeck coefficient of material j at reference temperature T_{ref} . The reference temperature considered is the room temperature (298 K). Substituting Eq. (18) into Eq. (13), we obtain the Seebeck coefficient of device at temperature T :

$$\alpha_{pn}(T) = (\alpha_p^{\text{ref}} - \alpha_n^{\text{ref}}) + (\mu_p - \mu_n) \ln\left(\frac{T}{T_{\text{ref}}}\right) \quad (19)$$

We solve the transient system of governing equations, Eqs. (1)–(3) and (15)–(17), simultaneously using an explicit forward differential approximation in time and a central difference scheme for evaluating the spatial gradients. Numerical simulations are performed to determine the temperature and electric current as a function of time.

2.6. Convergence

The time step size that ensures convergence for parabolic PDEs is as follows[22]:

$$\max(\Delta t) < \frac{\rho_j C_j \Delta x^2}{2k_j} \quad (20)$$

where Δt and Δx are time step size and mesh size, respectively. For the TEG elements, this time step resolves to approximately 28 μs for the mesh size chosen. Fig. 2 shows the effect of spatial mesh discretization and the time step on the convergence of temperature fields. Four time steps and mesh densities are shown in the figure. A time step of 50 μs and spatial grid spacing of 50 μm are selected for further analysis is sufficient to simulate the model with reliable accuracy while saving computational time. For this grid size, the relative error is less than 0.1% compared to the finer time step and mesh sizes (20 μs and 30 μm).

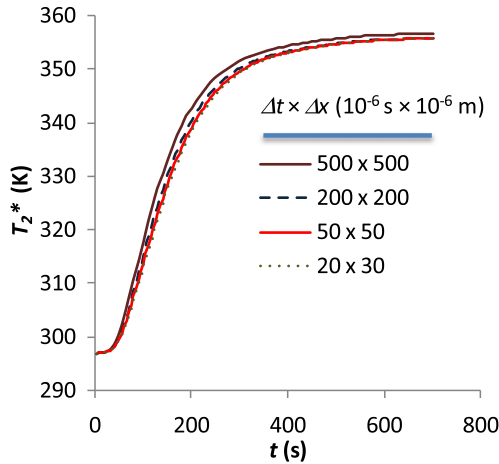


Fig. 2. Temperature at the top surface of the cold plate computed with four grid sizes.

3. Experimental analysis

An experimental setup was designed to establish parameters required for simulating the performance of the TEG and to validate the model. Fig. 3 shows the schematic of the experiment with a TEG (CUI Inc., model CP85438) on top of a heat source (Corning digital hot plate, model PC400-D). The source temperature was measured by a K-type thermocouple with diameter of 2 mm placed underneath the TEG. The thermocouple is sealed by conductive thermal grease to assure uniform heat distribution on the TEG hot surface. The top surface of the TEG is cooled by natural convection with a no heat sink. The TEG has ceramic hot and cold plates made of alumina (Al_2O_3) sandwiching the p–n thermo-elements. It is also sealed on all the sides by silicone rubber. The temperature of the top surface (the cold side) of the TEG, T_2^* , is detected by an infrared sensor mounted above the heater. Remote sensing with the infrared sensor does not disturb the natural convection on the cold surface.

Initially, the system is at room temperature (measured as 298 K) and the hot plate was switched on with a target temperature of 388 K (115 °C). The transient temperatures at the hot and cold surfaces of the TEG and the output voltage were recorded simultaneously into a digital computer using a data acquisition system (National Instruments-6009). The data acquisition was set at a rate of 0.5 s for about 700 s at which time the system attains a steady

state. Fig. 3b shows the schematic of various elements in the thermal conduction chain. The p- and n- thermo-elements, alumina hot and cold plates, the heater base plate and the contact resistance between the heater base plate and the TEG are all modeled for proper correlation between experimental and simulation results.

Experimental data are shown in Fig. 4. In Fig. 4, the temperatures measured on the actual thermoelectric generator and generated power (VI) calculated from output voltage are presented for four cases: in open-circuit (represented by load resistance, $R_0 = \infty$: inf), in closed-circuit, and four load resistance values: $R_0 = 10$, $R_0 = 1.5$, $R_0 = 0.5$ and $R_0 = 0.05 \Omega$, respectively. Fig. 4a shows the temperature at the hot and cold sides for all four cases (left axis) and the temperature difference – ΔT (right axis). The temperature difference is shown only for one case ($R_0 = 0.05 \Omega$). Due to the low current flowing through the circuit (the maximum value is about 0.04 and 0.07 A for $R_0 = 1.5$ and $R_0 = 0.05 \Omega$, respectively), the Thomson and Joule effects are not identifiable from the temperature fields. The electrical output, however, is strongly coupled to both the thermal behavior and the load resistor value. The generated power increases to a maximum but then decreases to reach a steady state. The power generation is highest when the load resistance value is close to the internal resistance, which is measured to be about 1.5 Ω . This observed experimental behavior is in agreement with trends reported in the earlier literature.

4. Material property determination

The TEG behavior simulation requires several material properties to be estimated for thermal, electrical and thermoelectrical behavior. The geometric parameters and properties of ceramic hot and cold plates are determined from either the manufacturer's data sheets or by direct measurements. For the alumina (Al_2O_3) plates, the properties were obtained from an online source for 96% alumina. The properties for the p- and n- thermo-elements were obtained from the literature. Geometric parameters and material properties used in the model are given in Table 1 for a single TEG cell.

To convert data obtained from a TEG with several cells into that for a single cell, the number of p–n pairs counted in the actual thermoelectric generator and their parallel/serial network connections are determined. The voltage results from the model are converted to the complete TEG response with the assumption that all p–n cells are operating under the same conditions. With N p–n

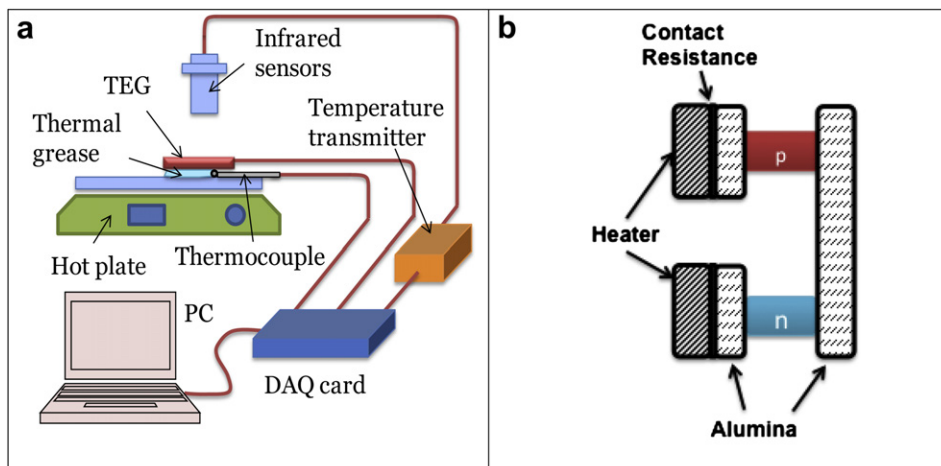


Fig. 3. (a) Schematic of the experimental setup. (b) model used.

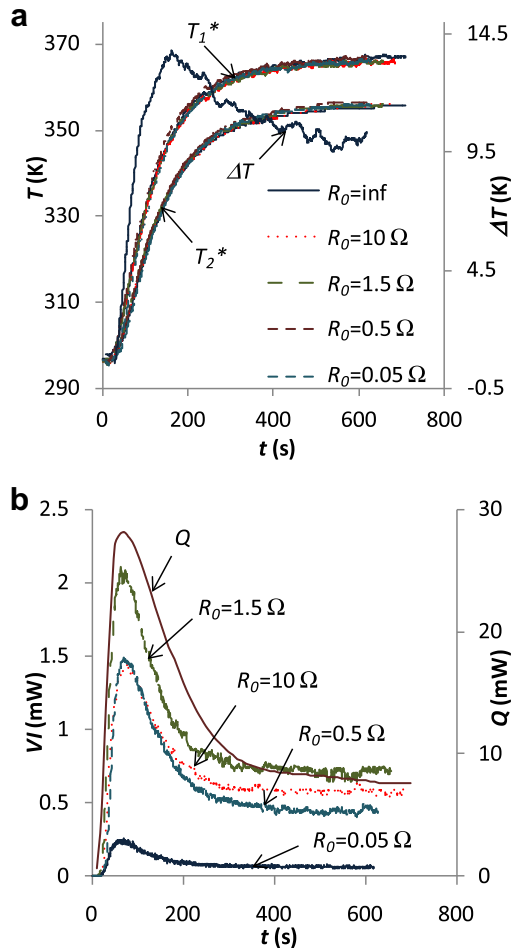


Fig. 4. (a) Temperatures at both sides and their difference and (b) output power obtained from the TEG. Input heat flux is shown for comparison.

Table 1
Properties of thermoelectric elements for a single TEG cell.

Parameters	Value	Unit	Source
L	2.2	mm	Measured
L_1	0.8	mm	Measured
L_2	0.8	mm	Measured
A_p	2.25×10^{-6}	m^2	Measured
A_n	2.25×10^{-6}	m^2	Measured
N	127		Measured
A_s	1.26×10^{-5}	m^2	Measured
A_1	1.26×10^{-5}	m^2	Measured
A_2	1.26×10^{-5}	m^2	Measured
ρ_p	7700	kg/m^3	[20]
ρ_n	7700	kg/m^3	[20]
ρ_1	3960	kg/m^3	[23]
ρ_2	3960	kg/m^3	[23]
h	2.5	$J/m^2 K$	[24]
μ_p	45	$\mu V/K$	Estimated
μ_n	-27	$\mu V/K$	Estimated
α_p^{ref}	25	$\mu V/K$	Estimated
α_n^{ref}	-32	$\mu V/K$	Estimated
ε_p	12	$\mu\Omega m$	[26]
ε_n	10	$\mu\Omega m$	[26]
k_p	1.8	$W/m K$	[25]
k_n	2.2	$W/m K$	[25]
k_1	18	$W/m K$	[23]
k_2	18	$W/m K$	[23]
C_p	200	$J/kg K$	[20]
C_n	200	$J/kg K$	[20]
C_1	880	$J/kg K$	[23]
C_2	880	$J/kg K$	[23]

cells electrically connected in series in the TEG ($N = 128$ for the TEG considered here), the relationship for electric quantities between the actual and the single TEG cell are in Eqs. (21)–(23):

$$V_{emf}^{act} = NV_{emf}^{single} \quad (21)$$

$$I^{act} = I^{single} \quad (22)$$

$$R_0^{act} = NR_0^{single} \quad (23)$$

By matching the transient theoretical results with the experimental data in open electrical circuit, the thermal and electrical properties of the TEG can be characterized. After the characterization process, the two results are compared in closed-circuit with different load resistance and in different applied heat flux conditions. In the first subsection, the effect of Thomson coefficients is discussed.

The effect of Thomson coefficients on the temperature and electric power output predictions is shown in Fig. 5. The temperature and voltage predictions are for closed-loop circuits with 10Ω and 1.5Ω load resistors. Fig. 5a and b shows that the temperature predictions are not significantly affected by the Thomson effect term but the output voltage/current is considerably impacted. Without Thomson effect, the predicted voltage is lower 20% than the cases with the presence of the Thomson coefficient. Inclusion of the Thomson effect with characterization of the Thomson

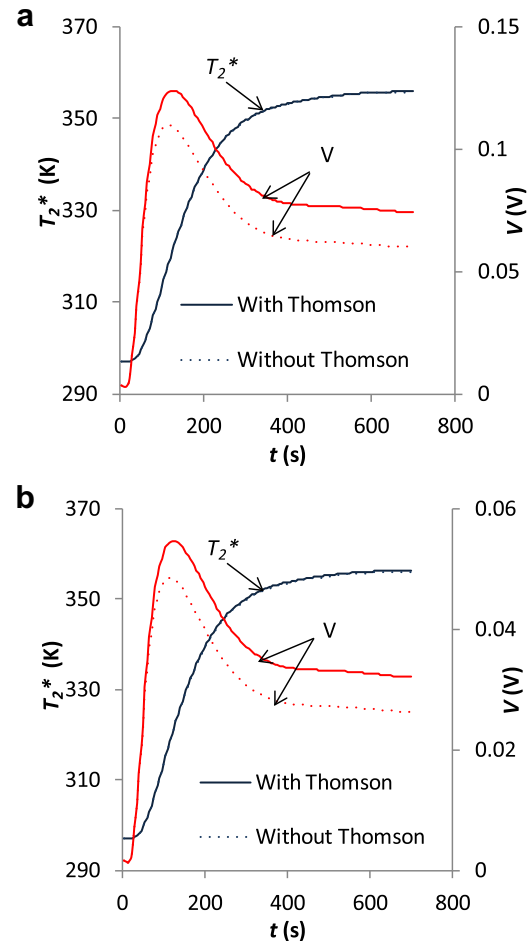


Fig. 5. Comparison results with and without Thomson coefficients for (a) $R_0 = 10 \Omega$ and (b) $R_0 = 1.5 \Omega$.

coefficient is critical for TEG models predicting power generation characteristics.

4.1. Thermal behavior

Since the heating rate of the hot plate used in the analysis cannot be measured with considerable accuracy due to contact and radiation losses, the temperature at the bottom surface of the TEG can be accurately measured by a thermocouple and translated to the model as a time-dependent input condition. The thermocouple is read using a high frequency data acquisition system.

The thermal characterization is conducted under open-circuit conditions in which V_{emf} is measured along with both the hot and cold temperatures. In this case, the non-linear coupling terms are negligible in the equations because the electric current in the circuit vanishes and the system consists of only the thermal diffusivity, Seebeck, and Thomson terms. Simulations are performed by varying the conductivity of p-type material (k_p) from 0.9 to 3.6 W/m K and that of the n-type material (k_n) from 1.1 to 4.4 W/m K. This range spanned 50–200% of the reported values for the conductivity of the TEG elements. Fig. 6 shows that both the transient and steady state behavior of the TEG being tested matches well with $k_p = 1.8$ W/m K and $k_n = 2.2$ W/m K. These values are typical for Bi_2Te_3 elements and such values are often reported in the literature. Note that the simulations included the contact resistance and heating plate inertia. Cheng et al. [20] identified that the specific heat capacities of elements (C_p and C_n) range from 154 to 210 J/kg K and that p-type and n-type elements have similar properties. In this analysis, the specific heat capacities of two materials are assumed constant and equal to 200 J/kg K. The density value for the TEG elements is set to 7700 kg/m³ based on the data identified from the literature.

4.2. Thermoelectric coupling

After the thermal properties are determined, the open-circuit experiment data for the V_{emf} are used to characterize the Seebeck and Thomson coefficients. Fig. 7a shows different voltage curves for different values of Seebeck coefficients while keeping the Thomson coefficients constant. The absolute value of Seebeck coefficients were varied in the range from 20 to 100 $\mu\text{V/K}$ and keeping the

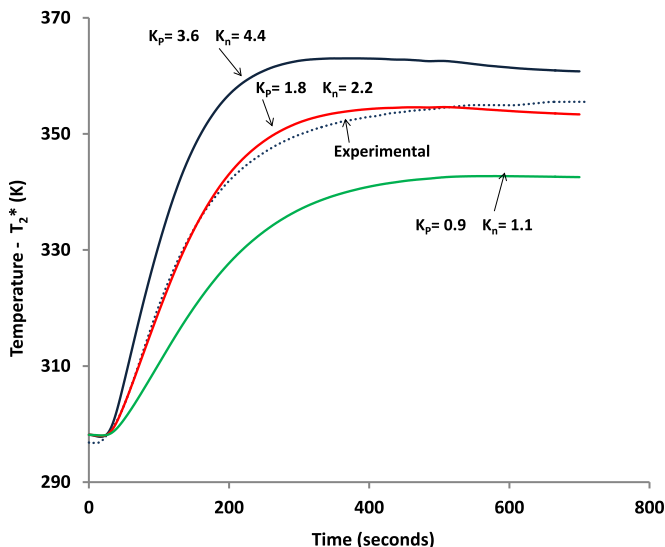


Fig. 6. Characterization of thermal conductivity with parametric analysis.

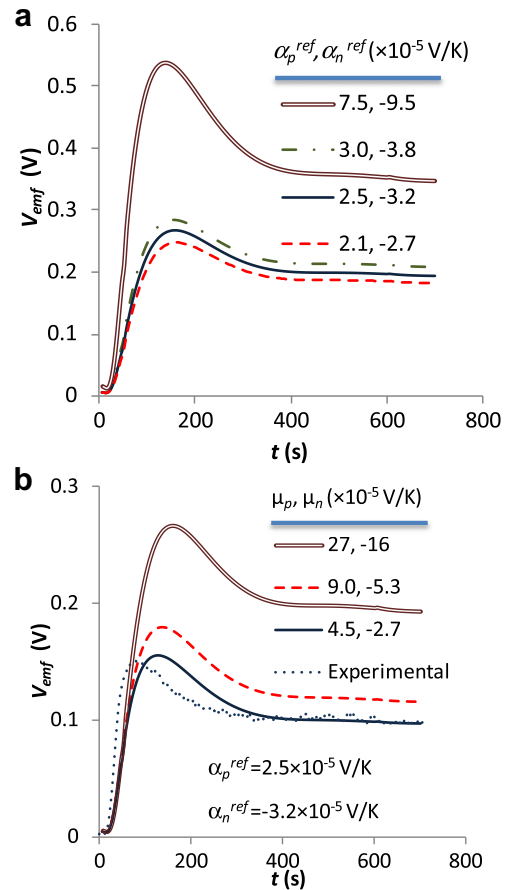


Fig. 7. Open-circuit characterization of Seebeck and Thomson coefficients.

Thomson coefficients constant. The Seebeck coefficients are estimated based on correlation of open-circuit voltage predictions and experimental observations. Fig. 7b shows the comparison of the experimentally observed voltage behavior and the predicted behavior when Thomson coefficients are varied. The Thomson coefficients of two thermo-elements are varied and the best voltage characteristic match occurs at $\alpha_p^{ref} = 2.5 \times 10^{-5}$, $\alpha_n^{ref} = -3.2 \times 10^{-5}$, $\mu_p = 4.5 \times 10^{-5}$ and $\mu_n = -2.7 \times 10^{-5}$ V/K. These values are used for closed-circuit behavior prediction and validation of the simulation results. These values differ from reference values in reference impurities, effects of wire leads and contact resistances. Both the peak voltage and the steady state values of the theoretically predicted and experimentally observed data are correlated with the set of material property parameters characterized with the open-circuit experiment.

4.3. Electrical properties

Next, we establish that the electrical resistivity of the TEG element matches that reported for Bi_2Te_3 . A closed-circuit test was employed in order to monitor the resistivity effect in output voltage. We pick the case with load resistor of 1.5 Ω . The resistivity values for the TEG as obtained from the literature are $\epsilon_p = 1.2 \times 10^{-5} \Omega\text{m}$ and $\epsilon_n = 1.0 \times 10^{-5} \Omega\text{m}$ [20]. Fig. 8 shows the correlation between the model predictions for various resistivity values and the experimentally generated closed-circuit voltage. The voltage response is seen to match reasonably with the resistivity values obtained from the literature. These values are adopted for all

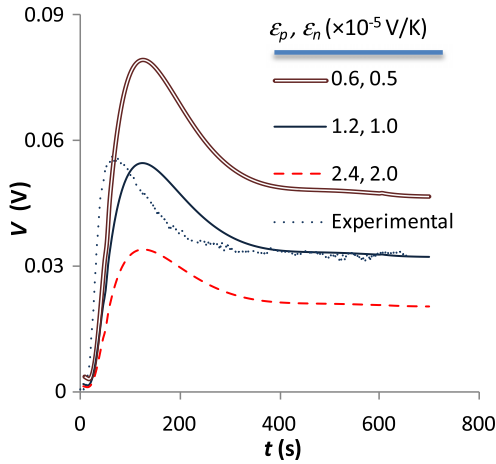


Fig. 8. Electrical resistivity characterization.

further analyses. We now use the theoretical model under applied heat source conditions with several load resistors to determine if the TEG behavior predicted by the model can be correlated with the experimental behavior.

5. Correlation of simulations with experiments

Fig. 9a–d shows both the experimentally measured data and simulation results from coupled thermo-electric model. In this correlation, we captured the time-dependent heat flux applied to the TEG into the simulation by imposing the temperature profile seen in Fig. 9a as a Dirichlet boundary condition on the hot side. The match of temperatures in Fig. 9a was therefore forced and the temperature profiles obtained experimentally and through simulation are then compared. Fig. 9b shows very good

correlation between both prediction and the observations. The temperature difference (ΔT) is also seen to match with time in Fig. 9c, indicating that the thermal inertia in the problem has been properly modeled. Fig. 9d shows a comparison between the open-circuit voltage measured and that predicted by the simulation. The simulation is seen to capture the voltage development trend during the transient as well as the steady state voltage output. Quantitatively, the peak voltage predicted differs by about 20%.

The TEG was then placed in closed-loop for power generation mode across resistive loads. Three load resistors were tested. Three load resistors of 10 Ω , 0.5 Ω and 1.5 Ω were selected. The current generated by a TEG is expected to be maximum when the internal resistance of the TEG equals the external load resistance. Fig. 10 shows the simulated and experimental temperature and voltage drop characteristics across the TEG element for the three load resistance cases. The results show that predicted and the experimental transient temperature profiles and output voltage match closely for both the cases. Slight difference in output voltage with the 0.5 Ω resistance is observed showing an effect of lead wires and contact resistance in the experiment. Generally, both the steady state and peak voltage values correspond very well. The close match of the peak and steady state values indicate accurate characterization of both the thermal conductivity and the thermoelectric properties of the device. Any contact resistance values are lumped into the thermal resistance and the electrical resistance of the materials. The voltage generated with the 10 Ω resistor is much higher than that of the 0.5 Ω , indicating the order of the magnitude of the internal resistance of the system. Therefore, it is critical to change the number and configuration (number of units in parallel vs. serial) of Seebeck elements to match the electrical resistance of the load connected to the TEG. Another experiment was carried out with the same TEG but at a higher hot plate setting temperature of 433 K (160 °C) and a load resistance of 1.5 Ω . Fig. 10c shows the cold side temperature rise with time. A close match between the

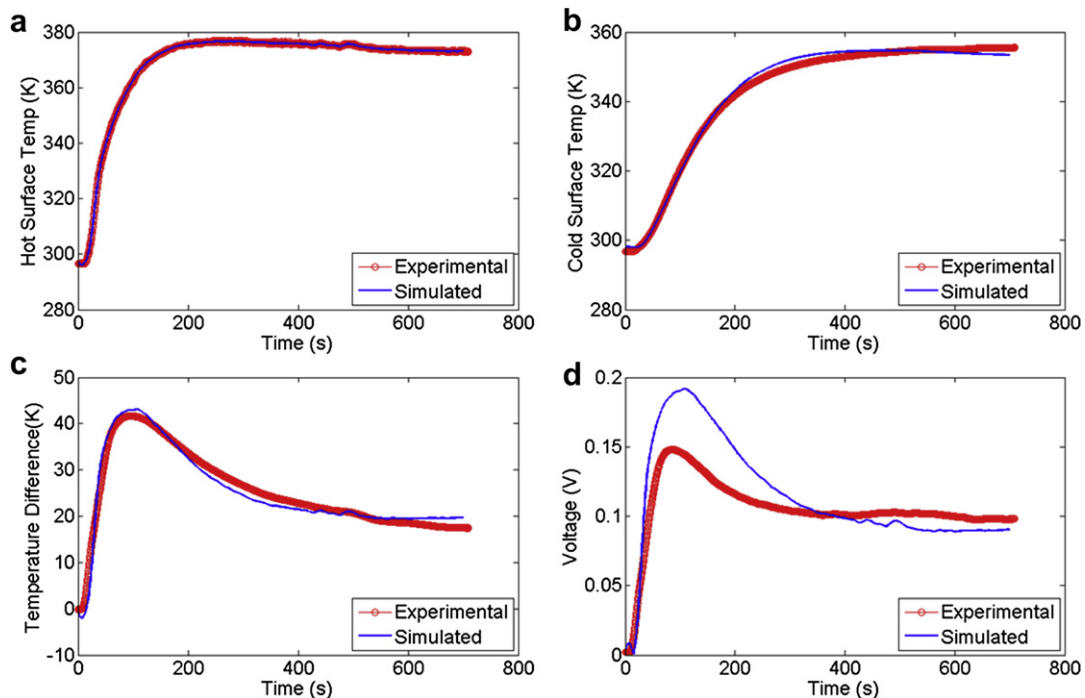


Fig. 9. Correlation of simulated and experimental behaviors of the TEG element. (a) Hot Side temperature profile is matched between the simulation and experiment. (b) Cold side temperature profile correlation. (c) Temperature difference between hot and cold sides. (d) Open-circuit voltage correlation.

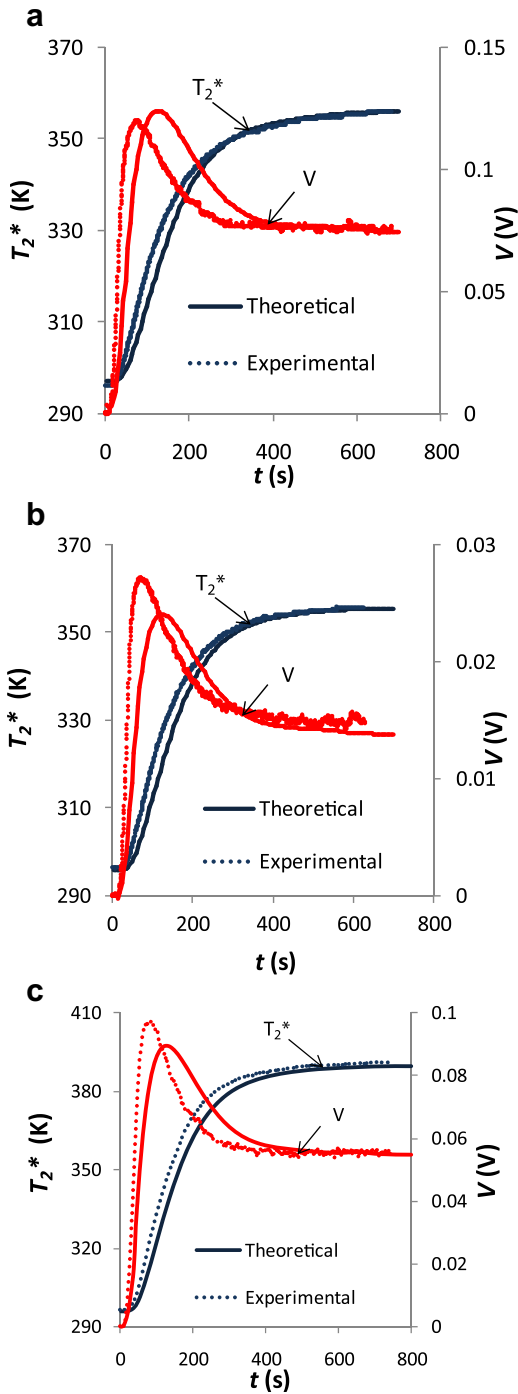


Fig. 10. Correlation between predictions and experimental observations (a) $R_0 = 10 \Omega$ and (b) $R_0 = 0.5 \Omega$ (c) $R_0 = 1.5 \Omega$.

predictions and experiments is also observed for both temperature and voltage curves in all cases.

6. Summary and concluding remarks

A coupled formulation of the thermoelectric behavior of a TEG with Seebeck, Peltier, Thomson and Joule effects included in both the thermal balance and the voltage predictions is developed and used to determine the power output characteristics of a TEG. Heat input represented by temperature is applied to one junction of the

TEG while the other junction is exposed to the environment under natural convection conditions. These conditions are typical in an energy harvesting application in which waste heat may be converted into a useful electrical energy. Finite-difference technique is used to compute the transient temperature and voltage profiles in the TEG when connected to a load resistor. In contrast to a thermoelectric cooler, for this problem, both the current flowing through the circuit and the temperature profiles are coupled and time-dependent and hence must be solved simultaneously.

Using the model, we determine the effect of the Thomson coefficients on the temperature distributions and the power output. While the effect is insignificant in the thermal domain, the power generation is impacted significantly by the Thomson term. In the present study, the current is low enough that the impact of the Joule heating term is minimal.

We used an open-loop experiment in which the TEG was subjected to a known temperature profile; several parameters for the material behavior model were established. The parameters whose ranges established from literature review were fine-tuned with the experimentation. Model predictions for closed-loop power generation scenarios correlate very well with the experimental analyses.

The peak voltage generation of the TEG subjected to a heat source on one boundary and natural convection to atmosphere on the other is not at the steady state. The steady state voltage is nearly half of the peak voltage delivered by the device. Therefore, the optimal operating point for these devices is not at the steady state but at the point of the highest temperature differential. In a power generation scenario, the heat input to the device must be controlled to hold the temperature differential at this optimal point. Design of such a controller requires accurately modeling the system behavior using a simulation framework as outlined in this paper.

Acknowledgements

Portions of this work were conducted with support from US/ ARMY ARDEC Contract: W15QKN-05-D0011-0051. Authors gratefully acknowledge the support.

References

- [1] S.B. Riffat, X. Ma, Thermoelectrics: a review of present and potential applications, *Applied Thermal Engineering* 23 (8) (2003) 913–935.
- [2] S.S.L. Chang, *Energy Conversion*, Prentice-Hall, Inc., Englewood Cliffs, NJ, 1963 (Chapter 3).
- [3] G.S. Nolas, J. Sharp, H.J. Goldsmid, *Thermoelectrics: Basic Principles and New Materials Developments* (2001).
- [4] Y. Yang, X.J. Wei, J. Liu, Suitability of a thermoelectric power generator for implantable medical electronic devices, *Journal of Physics D: Applied Physics* 40 (18) (2007) 5790–5800.
- [5] C. Wu, Analysis of waste-heat thermoelectric power generators, *Applied Thermal Engineering* 16 (1) (1996) 63–69.
- [6] Y.Y. Hsiao, W.C. Chang, S.L. Chen, A mathematic model of thermoelectric module with applications on waste heat recovery from automobile engine, *Energy* 35 (3) (2010) 1447–1454.
- [7] X. Gou, H. Xiao, S. Yang, Modeling, experimental study and optimization on low-temperature waste heat thermoelectric generator system, *Applied Energy* 87 (10) (2010) 3131–3136.
- [8] R. Yang, et al., Transient cooling of thermoelectric coolers and its applications for microdevices, *Energy Conversion and Management* 46 (9, 10) (2005) 1407–1421.
- [9] S. Angrist, *Direct Energy Conversion*, fourth ed., Allyn and Bacon, Inc., Boston, MA, 1982 (Chapter 4).
- [10] P. Ziolkowski, et al., Estimation of thermoelectric generator performance by finite element modeling, *Journal of Electronic Materials* (2010) 1–10.
- [11] L. Chen, et al., Effect of heat transfer on the performance of thermoelectric generators, *International Journal of Thermal Sciences* 41 (1) (2002) 95–99.
- [12] D. Ebling, et al., Multiphysics simulation of thermoelectric systems for comparison with experimental device performance, *Journal of Electronic Materials* 38 (7) (2009) 1456–1461.
- [13] J. Xie, C. Lee, H. Feng, Design, fabrication, and characterization of CMOS MEMS-based thermoelectric power generators, *Journal of Microelectromechanical Systems* 19 (2) (2010) 317–324.

- [14] M. Chen, et al., Transient behavior study of thermoelectric generators through an electro-thermal model using SPICE, In: International Conference on Thermoelectrics, ICT, Proceedings (2006).
- [15] E.E. Antonova, D.C. Looman, Finite elements for thermoelectric device analysis in ANSYS, In: International Conference on Thermoelectrics, ICT, Proceedings (2005).
- [16] D. Mittrani, et al., One-dimensional modeling of TE devices considering temperature-dependent parameters using SPICE, *Microelectronics Journal* 40 (9) (2009) 1398–1405.
- [17] P.E. Gray, *The Dynamic Behavior of Thermoelectric Devices*, John Wiley & Sons, Inc., New York, 1960 (Chapters 2–4).
- [18] D. Astrain, et al., Study of the influence of heat exchangers' thermal resistances on a thermoelectric generation system, *Energy* 35 (2) (2010) 602–610.
- [19] D.T. Crane, An introduction to system level steady-state and transient modeling and optimization of high power density thermoelectric generator devices made of segmented thermoelectric elements, *Journal of Electronic Materials* 40 (5) (2011) 561–569.
- [20] C.H. Cheng, S.Y. Huang, T.C. Cheng, A three-dimensional theoretical model for predicting transient thermal behavior of thermoelectric coolers, *International Journal of Heat and Mass Transfer* 53 (9, 10) (2010) 2001–2011.
- [21] W. Seifert, M. Ueltzen, E. Mueller, One-dimensional modelling of thermoelectric cooling, *Physica Status Solidi (A) Applied Research* 194 (1) (2002) 277–290.
- [22] Chapra, S.C. and R.P. Canale, *Numerical Methods for Engineers*, fifth ed., 2005, New York: McGraw-Hill.
- [23] www.Matweb.com, Materials Properties data.
- [24] F.P. Incropera, D.P. Dewitt, *Fundamentals of Heat and Mass Transfer*, fourth ed., John Wiley & Sons, Inc., New York, 1996.
- [25] D.M. Rowe, *CRC Handbook of Thermoelectrics*, CRC: Press, USA, 1995, pp. 145–230.
- [26] K.H. Lee, O.J. Kim, Analysis on the cooling performance of the thermoelectric micro-cooler, *International Journal of Heat and Mass Transfer* 50 (9, 10) (2007) 1982–1992.